Erschienen in: Solar Energy Materials and Solar Cells. 2018, 187, S. 104-112
https://doi.org/10.1016/j.solmat.2018.07.024

Multi-characterization study of interface passivation quality of amorphous sub-stoichiometric silicon oxide and silicon oxynitride layers for photovoltaic applications

Jonathan Linke[a], Maria Antonietta Fazio[b], Daniela Cavalcoli[b,*], Barbara Terheiden[a]

[a] *Department of Physics, University of Konstanz, Germany*
[b] *Department of Physics and Astronomy, University of Bologna, Italy*

A R T I C L E I N F O

Keywords:
Silicon passivation
Amorphous silicon
SiO_xN_y
SiO_x
FTIR
Spectral ellipsometry
SPV
PCD

A B S T R A C T

Si solar cells have achieved a world record efficiency of 26.7% as a result of both improvement of Si ingot growth and optimal passivation of surfaces and interfaces. In this framework, a clear understanding of the electronic, optical, structural and passivation properties of innovative Si based layers is mandatory. The present study reports on the characterization of amorphous sub-stoichiometric silicon oxide (a-SiO_x) and silicon oxynitride (a-SiO_xN_y) layers and their surface passivation properties. The layers have been deposited on float zone Si wafers (2 Ω cm, (100)-oriented, 250 µm thick) by plasma enhanced chemical vapour deposition (PECVD) adding increasing fractions of N_2O and CO_2 to the SiH_4 flux during deposition to increase the energy band gap of the layers. Composition, optical properties, light induced electronic transitions and minority carrier lifetimes of Si wafers passivated with these layers have been investigated by Fourier-transform infrared spectroscopy (FTIR), spectral ellipsometry, surface photovoltage (SPV) spectroscopy and photo conductance decay (PCD). The overall characterization of the layers has allowed us to understand the effect of increasing N_2O and CO_2 flux ratios during deposition on the interface properties. The present study establishes the importance of the approach of using multiple characterization methods in the evaluation of the passivation capability of layers that combine large optical band gap and surface passivation.

1. Introduction

The energy conversion efficiency of single-crystalline silicon solar cells has improved steadily over the last decades and has recently reached a world record efficiency of 26.7% [1]. In parallel, the increased production volumes and associated maturity of the technology have reduced the cost of photovoltaic modules so far that solar photovoltaic electricity has already reached grid parity in many countries and locations [2]. Such a strong enhancement of this technology is a consequence of the improvement of silicon ingot growth processes and the control of defects and contamination during solar cell fabrication. The bulk electronic quality of crystalline silicon wafers has improved to such a point that further device advances now rely on innovative surface passivation schemes. To achieve a high efficiency in silicon based solar cells an excellent control of interfaces must be adopted.

Intrinsic a-Si:H films have been known for some decades as effective passivation layers via chemical surface states passivation. Doping of these films as typically applied in Si heterojunction (SHJ) cells causes an additional field effect passivation, but it diminishes the surface state passivation at the interface. In order to improve the interface passivation, a few nm thick buffer layer of intrinsic a-Si:H is inserted between the c-Si substrate and the doped film. This strategy has led Sanyo, now Panasonic, to achieve high efficiency SHJ cells [3].

Recently, the role of surface passivation on the final efficiency of SHJ solar cells has been shown by Yoshikawa et al. [4]. These authors produced an inter-digitated contact (IBC) SHJ cell with a certified efficiency larger than 26% through careful optimization of optical and passivation properties and efficient carrier collection on the front side of the cell. Notwithstanding these high efficiencies achieved by SHJ cells, a-Si:H films present high parasitic absorption of light, causing a loss in short circuit current, and high series resistance, causing a reduction in fill factor. The absorption within the a-Si:H films can be minimized by widening the optical band gap, for example through the incorporation of carbon, nitrogen or oxygen in the amorphous matrix

* Correspondence to: Physics and Astronomy, Dept University of Bologna, viale C Berti Pichat 6/II, 40127 Bologna, Italy.
E-mail addresses: jonathan.linke@uni-konstanz.de (J. Linke), maria.fazio2@unibo.it (M.A. Fazio), daniela.cavalcoli@unibo.it, cavalcoli@bo.infn.it (D. Cavalcoli), Barbara.Terheiden@uni-konstanz.de (B. Terheiden).

Konstanzer Online-Publikations-System (KOPS)
URL: http://nbn-resolving.de/urn:nbn:de:bsz:352-2-nqa1iu0s2fus2

[5,6 and references therein], while the resistivity can be reduced through the incorporation of crystalline phases [7,8].

While the a-Si:H /c-Si interface passivation mechanisms have been investigated for at least one decade [9,10], this is not the case for a-Si:H with incorporation of small amounts of O and N, which we refer to as amorphous sub-stoichiometric silicon oxide (a-SiO_x) and silicon oxynitride (a-SiO_xN_y) layers. Even if these materials are already applied in fields different from photovoltaics, e.g. as buffer layers for organic based photodetectors [11] or as matrix layer for superlattices with Si nanocrystals [12,13], their fundamental properties have not yet been investigated in detail. These innovative passivating layers consist of complex non-stoichiometric compounds containing amorphous and crystalline phases and their properties vary substantially as a function of the deposition method and subsequent annealing processes. Beside the fundamental properties, the influence of the structure of the amorphous network on electron-hole recombination processes at surfaces and interfaces is also not clear yet. However, a detailed understanding of this interrelation is in turn a mandatory requirement for the optimization of the layers for the application as means of surface passivation of Si wafers.

The aim of the present work is the discussion of a multi-characterization approach focused on the study of structural and passivation properties of sub-stoichiometric a-SiO_x and a-SiO_xN_y layers on c-Si surfaces. The knowledge and optimization of these properties are mandatory in order to further improve SHJ solar cell efficiency.

Therefore, we deposited these layers from silane gas (SiH_4) and added varying fluxes of N_2O or CO_2 gas to the PECVD reactor to obtain a-SiO_xN_y and a-SiO_x layers, respectively. These layers have on one hand a beneficial effect as their optical gap is improved with respect to a-Si:H, but on the other hand a detrimental effect as high flux ratios of N_2O or CO_2 during deposition lead to an increase in surface recombination.

Several properties of these layers have been evaluated with multiple techniques to investigate the implication of the structure of the amorphous network at the interface on electron-hole recombination processes in dependence of the N_2O and CO_2 flux compositions. In detail, optical properties, light induced electronic transitions and minority carrier lifetimes of these layers have been examined by Fourier-transform infrared spectroscopy (FTIR), spectral ellipsometry, surface photovoltage (SPV) spectroscopy and photoconductance decay (PCD). The present study establishes the importance of this approach based on the use of multiple characterization methods in the evaluation of the passivation capability of layers that combine large optical band gap and surface passivation.

2. Materials and methods

The a-SiO_xN_y (N sample set) and a-SiO_x (C sample set) layers were deposited by PECVD on 250 µm thick boron-doped silicon float-zone material of an area of $5 \times 5\,cm^2$ ($2\,\Omega\,cm$, (100)-oriented) using a commercial tool (PlasmaLab 100 from Oxford Instruments) with a radiofrequency of 13.56 MHz. All the parameters were kept constant for all depositions (P = 100 W, p = 450 mTorr, T = 175 °C, electrode distance d = 20 mm, deposition duration t = 150 s) except for the gas fluxes. Additional to pure SiH_4 gas, either N_2O or CO_2 gas was added to the plasma. The dilution ratios of N_2O and CO_2 in silane are defined by $R_x = [X]/([X] + [SiH_4])$ with X = N_2O or CO_2 and the square brackets representing the gas fluxes. The ratios were varied in the range of 4.8–16.6% for N_2O and in the smaller range of 4.8–9.1% for CO_2, because each CO_2 molecule carries twice as many oxygen atoms as each N_2O molecule. A reference a-Si:H sample was deposited using pure SiH_4 gas only. The corresponding labelling of the samples and their flux ratios are listed in Table 1.

Immediately before each deposition, the samples were dipped in hydrofluoric acid solution (2%) to remove silicon oxide from the surfaces. The layers were deposited on both sides of each sample in separate depositions and immediately before the next sample was deposited, the deposition chamber was cleaned. Since the deposition duration was kept constant while the plasma composition was changed, the resulting layer thicknesses determined by spectral ellipsometry measurements are not equal but vary in the range from 100 to 140 nm. The passivation activation was achieved by annealing the layers on a hotplate in ambient air to 300 °C for 15 min.

Table 1
Labelling of the investigated samples, chosen to provide information about the gas flux ratio R_x used during deposition.

Sample (label)	R_{N2O} (%)	R_{CO2} (%)
N4.8	4.8	0
N9.1	9.1	0
N13	13	0
N16.6	16.6	0
C4.8	0	4.8
C7	0	7
C9.1	0	9.1
Reference	0	0

The microstructure of the layers as well as an estimate for incorporated nitrogen and oxygen was determined qualitatively with a FTIR setup (Vertex 80 from Bruker Optics) in terms of relative absorption strengths of selected bonds in the range of 500–2500 cm^{-1} with a resolution of 8 cm^{-1}. A baseline correction was applied to all spectra before multi-Gaussian fit procedures were performed on each of the two main absorption bands separately. The positions of the evaluated peaks as reported in the literature are depicted in Table 2. In order to compare the bond densities qualitatively, the relative absorption strength was determined by the ratio of the integral under the fitted Gaussian peak of interest and under the corresponding peak of a reference sample.

The refractive index variation within the layer as well as the layer thicknesses were determined using a Vertical VASE Rotating analyzer ellipsometer (J.A. Woollam Co., Inc.) operated in a spectral range of 500–2000 nm. The data (Ψ, Δ) were fitted by a graded Cauchy model, which considered the investigated layers as divided into 21 sublayers with fixed thickness, but individual homogeneous refractive indices to model variations of the optical constants within the layers, similarly to the approach in [19]. For the top surface a roughness layer was included in the model, which was simulated by an effective medium approximation of 50% layer material and 50% void.

Electronic transitions and effective minority carrier lifetimes were determined by SPV measurements of the light induced variation of surface or interface voltage, which is capacitively picked up in a metal-insulator-semiconductor configuration and amplified with a phase

Table 2
Literature values of the infrared active absorption peaks and corresponding bond vibrations of a-SiO_x and a-SiO_xN_y evaluated in this study.

Wavenumber [cm^{-1}] (from literature)	Bonds	Modes	Reference
640	Si-H / Si-H_2	wag / roll	[14]
780	Si-H / Si-O-Si	coupling of both bonds	[15]
840	Si-H_2	interaction between two Si-H_2 groups	[14]
850	Si-N	asymmetric stretch	[16]
890	Si-H_2	interaction between two Si-H_2 groups	[14]
980	Si-O-Si	asymmetric stretch	[15]
1107	O_i	interstitial oxygen	[17]
2000	Si-H	stretch	[18]
2100	Si-H_2 / Si-H_3	stretch	[18]

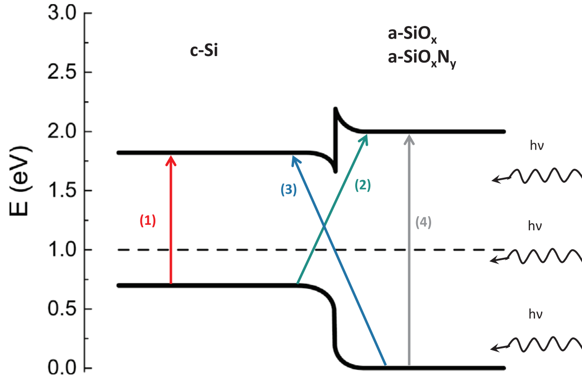

Fig. 1. Sketch of band diagram of a-SiO_x and a-SiO_xN_y layers. The possible electronic transitions under illumination are highlighted with numbers and arrows of different colors. A rough estimate of the band gap of 2 eV for the top layer has been used.

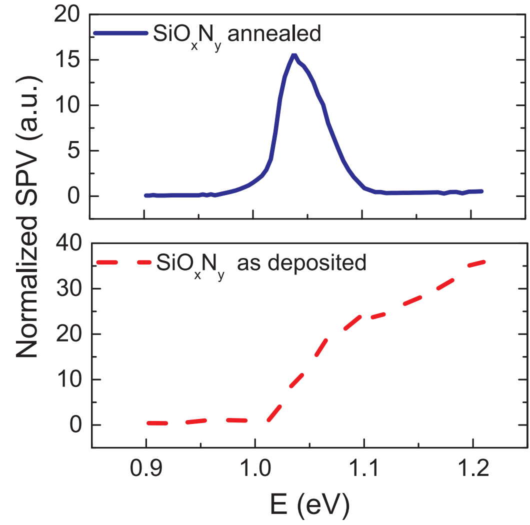

Fig. 2. SPV spectra measured with the QTH lamp SiO_xN_y samples annealed, blue, solid line, and as-deposited, red, dashed line. The recombination is linked to a decrease of the signal at higher photon energies (blue curve), while good passivation leads still to a higher signal (red curve). (For interpretation of the references to color in this figure legend, the reader is referred to the web version of this article.).

sensitive detector locked to the light chopping frequency. SPV spectra have been obtained using a laboratory-made apparatus described elsewhere [20] based on a 500M SPEX spectrometer. A Quartz Tungsten Halogen (QTH) as well as a short arc Xe lamp were used to inject photons in different spectral ranges. The SPV signal intensity was normalized to the photon flux and plotted as a function of the photon energy.

Two standard methods of analysing the spectra were used. In one method, a whole spectrum is evaluated at a fixed chopper frequency and in the other method the signal at a fixed photon energy is evaluated over several spectra under variation of the chopper frequency. In the following, the former method is referred to as SPV spectroscopy for determination of electronic transitions and the latter method is referred to as ac-SPV for estimation of effective minority carrier lifetimes.

In SPV spectroscopy, electronic transitions are detected as changes in the slope of the SPV spectra, which correspond to band-to-band transitions or intra-band transitions at the surface or interface of a multi-layered structure [21–23]. In order to clarify the expected transitions in the SPV spectra, in Fig. 1 the band diagram of the interface between the a-SiO_xN_y and a-SiO_x top layers (right) and the c-Si substrate (left) and the possible electronic transitions under illumination are sketched. For the top layer a lower limit of the band gap at 2 eV has been considered, while literature data show values ranging from 2 to 3 eV [5,6].

The highlighted transitions are listed as follows:

(1) band-to-band transition in the c-Si substrate at around 1.1 eV;
(2) transition from the c-Si valence band to the top layer conduction band at around 1.3 eV;
(3) transition from the top layer valence band to c-Si conduction band at around 1.8 eV;
(4) band-to-band transition in the top layer at around 2 eV.

The energies of the transitions shown in Fig. 1 are just a rough indication for the effective transitions that are observed by SPV spectroscopy, as the real band diagram will be more complicated due to the presence of amorphous phases and disorder in the layers.

Additionally, information about the passivation quality of the layers can be extracted from these SPV spectra as illustrated in Fig. 2, where nanocrystalline SiO_xN_y layers from previous publications [5,6] are presented, one with large interface recombination (top, annealed at 800 °C for 3 h) and one with low interface recombination (bottom, as-deposited). Both spectra show a knee at around 1.05–1.1 eV, related to the band-to-band transition in the c-Si substrate. Above this photon energy the signal does not decrease for the as-deposited sample, while it suddenly drops for the annealed one.

The inverse of the absorption coefficient, which equals the light penetration depth, substantially decreases for photon energies above the band gap and thus the SPV signal in this spectral region is strongly affected by recombination phenomena at the interface [22]. Since the decreasing trend of the SPV signal in the annealed sample is in this spectral region above the band gap, it can be related to strong electron-hole recombination at the interface, as confirmed by the observation of oxygen precipitates at the interface [7]. On the contrary, the SPV signal in the as-deposited sample does not decrease above the band gap, demonstrating better interface characteristics and lower interface recombination. Therefore, this experimental evidence clearly demonstrates the capability of the SPV spectroscopy to reveal the passivation quality of an interface.

In the case of the ac-SPV evaluation, the minority carrier lifetime of the samples can be extracted. Since the SPV signal is proportional to the number of photo-generated carriers at each chopper frequency, the lifetime related to an SPV feature, typically a peak or a knee at the band gap of the investigated layer, could be extracted by fitting the frequency dependent data at one photon energy with the following function [24–26]:

$$\mathrm{SPV} = \frac{A\tau}{(1+\omega^2\cdot\tau^2)^{1/2}} \tag{1}$$

where A is a proportionality constant, τ the effective minority carrier lifetime and ω the angular chopper frequency $\omega = 2\pi f$.

Further characterization of the passivation quality was carried out by measuring the effective minority carrier lifetime, evaluated at an excess carrier density of $\Delta n = 1\cdot10^{15}\ \mathrm{cm}^{-3}$, using a PCD tool (WCT 120 from Sinton Instruments Inc.). The relative error for this characterization method was fixed to 8% as suggested in [27,28].

3. Results and discussion

All samples have been analysed by FTIR, spectral ellipsometry, SPV spectroscopy and PCD to determine the relevant interface and surface properties of the silicon wafer and the a-SiO_xN_y and a-SiO_x layers.

3.1. Fourier-transform infrared spectroscopy

In the infrared absorption spectra two main bands were analysed

separately, namely the low frequency band (LFB) in the range of 550–1200 cm^{-1} and the high frequency band (HFB) in the range of 1950–2150 cm^{-1}. The LFB includes the absorption of hydrogen, oxygen and nitrogen bonds, while the HFB includes solely the absorption of hydrogen bonds. All observed peaks could be related to the bonds depicted in Table 2.

Surprisingly, no peak in the absorption spectra of the C sample set could be related to carbon bonds. In [29] the authors deposited similar layers with R_{CO2} between 0% and 50% and determined the carbon concentration. A rough linear fit of these results gives a carbon concentration of approximately $7{\cdot}10^{18}$ cm^{-3} or $1.4{\cdot}10^{-2}$ at% for R_{CO2} = 9.1% as the highest used flux ratio in the C sample set. It seems reasonable that such a low concentration does not exhibit absorption peaks in the FTIR spectra, but it may still influence the optical and electrical properties of the layers. However, all the following results are explained without the assumption of a significant carbon influence.

On the contrary, a broad absorption peak at 850 cm^{-1} has been detected in the N sample set which corresponds to the asymmetric stretching mode of Si-N [16] and thus a significant amount of nitrogen has been incorporated in the layers. Its relative absorption strength normalized to the absorption strength of the sample with the highest nitrogen content (N16.6) is increased by a factor of roughly six with increasing R_{N2O} from 4.8% to 16.6%, as presented in Fig. 3a.

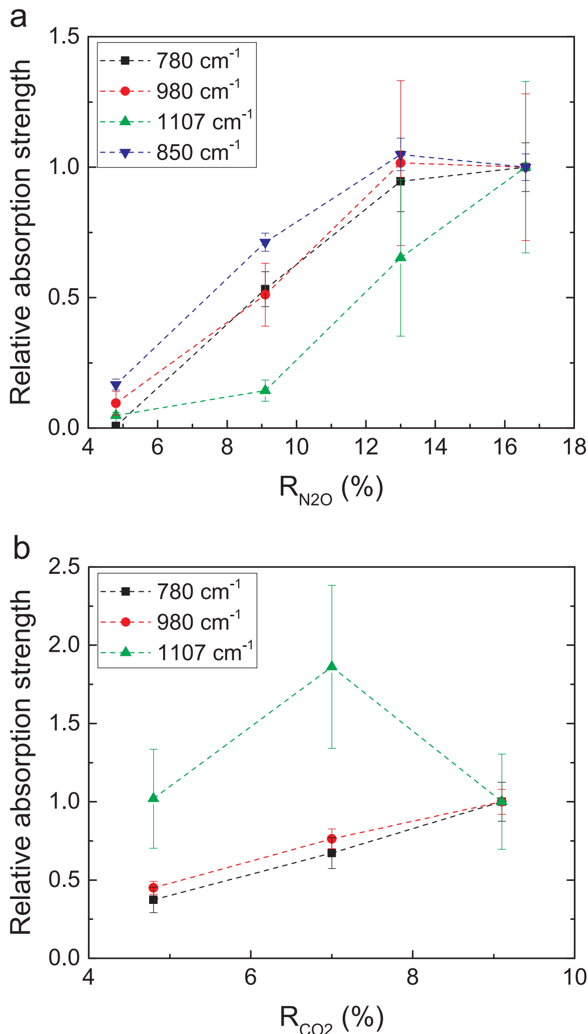

Fig. 3. Relative absorption strengths of all oxygen (780 cm^{-1}, 980 cm^{-1}, 1107 cm^{-1}) and nitrogen (850 cm^{-1}) bonds as depicted in Table 2 for a) the N sample set (normalized to the absorption strengths of N16.6) and b) the C sample set (normalized to the absorption strengths of C9.1).

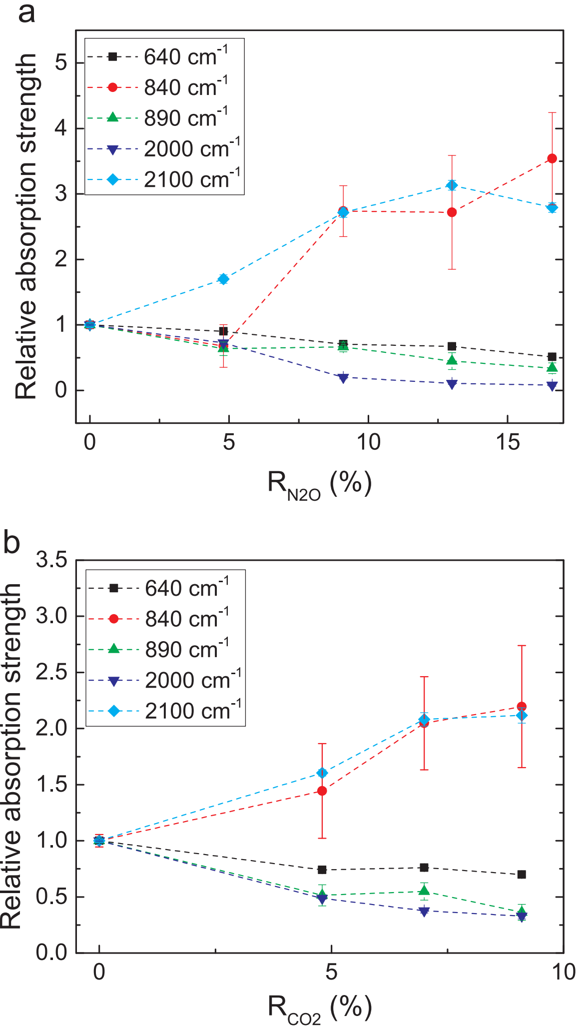

Fig. 4. Relative absorption strengths of all hydrogen bonds as depicted in Table 2, normalized to the absorption strengths of the reference sample, for a) the N sample set and b) the C sample set.

For the three oxygen peaks at 780 cm^{-1} (coupling of Si–H and Si–O–Si bonds [15]), 980 cm^{-1} (Si-O-Si asymmetrical stretching mode [15]) and 1107 cm^{-1} (interstitial oxygen [17]), the absorption strengths were normalized to the corresponding sample with the largest oxygen content (N16.6 or C9.1). In both sample sets, the relative absorption strengths increase simultaneously with increasing R_x, as can be seen in Fig. 3a,b. This suggests a similar increase in the oxygen concentration for both sample sets, as expected. It should be remarked, that the relative absorption strength of the peak at 1107 cm^{-1} shows no clear trend for the C sample set, which will be discussed in detail later.

The absorption strengths of the peaks corresponding to hydrogen bonds were normalized to the absorption strengths of the pure a-Si:H reference sample and are shown in Fig. 4 for both the N and C sample sets, which follow the same trends and thus they are discussed simultaneously.

The absorption peak at 640 cm^{-1} is caused by the wagging mode of Si–H bonds as well as by the rolling mode of Si–H_2 bonds and is therefore commonly used to quantify the total hydrogen content in the layer [18,30]. Its relative absorption strength is reduced with increasing R_x, meaning that the total hydrogen concentration is reduced.

The two peaks in the HFB can be identified with the stretching modes of Si-H (2000 cm^{-1}) and Si-H_2 / Si-H_3 (2100 cm^{-1}) bonds [18]. This identification is not completely clear and controversially discussed in the literature [30,31], especially by theoretical predictions of a finer

splitting in distinct modes below the typical resolutions of FTIR measurement devices [14].

Instead, following [32], we can assume that the increase of the fraction $\chi = I_{2100}/(I_{2000} + I_{2100})$ with I_{2000} and I_{2100} being the absorption strengths of the corresponding peak, is related to the increase of the disorder in the amorphous network. Such larger disorder can either be expressed by a larger number of silicon atoms with more than one dangling bond that can possibly be saturated by hydrogen atoms or by the presence of hydrogen bonded at inner surfaces of microvoids [30]. In both cases, the number of silicon atoms bond to two or more hydrogen atoms is increased.

Fig. 4 clearly shows that the relative absorption strength of the peak at 2000 cm^{-1} is reduced with increasing R_x, while the relative absorption strength of the peak at 2100 cm^{-1} is increased. This behaviour is also reflected in the fraction χ, which increases from an initial value of $\chi = 0.28$ for the pure a-Si:H reference sample to a value of 0.93 for the sample N16.6 and a value of 0.72 for the sample C9.1. As stated above, this increase in the fraction χ is accompanied by an increase in the Si–H_2 bond density.

The two absorption peaks at 840 cm^{-1} and 890 cm^{-1} appear as a doublet and are a result of interactions of two Si-H_2 groups. They typically appear for larger hydrogen concentrations when the distance of such two groups is comparably small [14]. The peak at 840 cm^{-1} is weak for low hydrogen concentrations, but it becomes higher than the peak at 890 cm^{-1} as the Si–H_2 bond density is increased.

This effect can be clearly observed in Fig. 4 where the relative absorption strength of the peak at 840 cm^{-1} increases with increasing R_x up to a factor of 3.5, while the relative absorption strength of the peak at 890 cm^{-1} decreases at the same time to one-third of the reference value. However, this finding would be unexpected if linked to the hydrogen concentration, since the overall hydrogen content is decreased as concluded from the relative absorption strength reduction of the peak at 640 cm^{-1}. It should instead be considered as a result of the higher Si–H_2 bond density as concluded from the increase of the fraction χ.

In summary, the FTIR analysis revealed a general similarity between the N and C sample sets in terms of an increasing disorder of the amorphous network with increasing flux ratios R_x, accompanied by increased Si–H_2 and Si–H_3 bond densities and by the probable formation of microvoids.

3.2. Spectral ellipsometry

The spectral ellipsometry data have been fitted with the model described in Section 2 to determine variations of the optical constants within the layers of the N and C sample sets. In Fig. 5 each data point represents the refractive index at a wavelength of 600 nm of one of the 21 sublayers of the fitted model. For the reference sample the refractive index is approximately constant over the whole range of the layer, except for the first sublayer at the interface to the substrate, where the refractive index is significantly lowered. Following this observation, we distinguish between the refractive index at the interface to the substrate and the “steady-state” refractive index, which evolves far from the interface.

The reduction of the refractive index close to the substrate is observable for all the samples, while for larger flux ratios R_x this lowering takes place even at a distance of a few sublayers from the substrate. The reduction in the refractive index of amorphous silicon layers can be attributed to a less dense microstructure [33]. Hence, the lower refractive index at the interface might be caused by an initial island growth of the deposition, which has not yet reached the steady state growth. Following this explanation, the density of the amorphous network at the interface to the substrate decreases with increasing R_x, probably accompanied by microvoid formation, as the region of this microstructure variation measured in distance from the substrate is increased simultaneously.

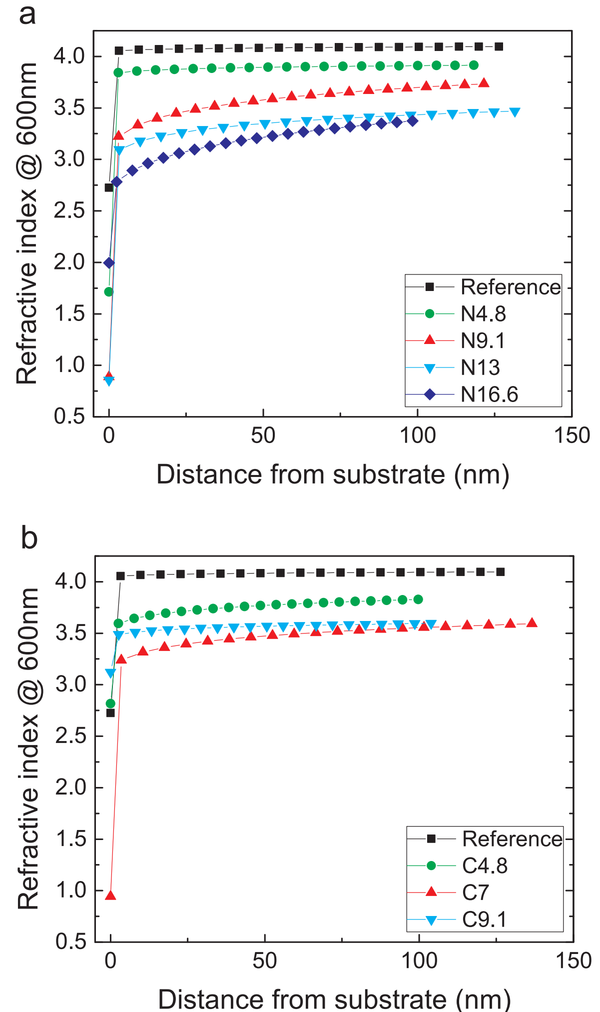

Fig. 5. Refractive index variation at a wavelength of 600 nm as function of the distance from the substrate for a) the N sample set and b) the C sample set. Each data point represents the refractive index in one of the 21 sublayers, which were used to fit the ellipsometry data.

Apart from this variation of the refractive index along the distance from the substrate, the steady-state refractive indices of the N sample set are larger than 3 and larger than 3.3 for the C sample set. At the wavelength of 600 nm, stoichiometric silicon oxide (SiO_2) has typically a refractive index of around $n_{SiO2} = 1.5$ and stoichiometric silicon nitride (Si_3N_4) of around $n_{Si3N4} = 2.0$ [34]. Since the measured refractive indices are closer to the refractive index of the pure a-Si:H reference sample of roughly 4.0, the layers of both sample sets have to be considered strongly sub-stoichiometric.

Having a closer look at the steady-state refractive index reveals that it decreases with increasing R_{N2O} in the N sample set as can be seen in Fig. 5a. This behaviour could be explained by an increasing oxygen content in the layers with increasing R_{N2O}, as qualitatively described before in the discussion of the FTIR results (Section 3.1). Surprisingly, this expected trend is not that clear for the C sample set. The sample C7 shows a lower “steady-state” refractive index than sample C9.1 and it has a much stronger reduction of the refractive index in the sublayer at the interface than the other C samples. A similar deviation is observable in the FTIR absorption peak of interstitial oxygen at 1107 cm^{-1}, where the relative absorption strength of the sample C7 is increased by a factor of two compared to the other C samples, but not in the other two oxygen absorption peaks (see Fig. 3b), suggesting an increased amount of interstitial oxygen. The presence of more interstitial oxygen can be related to the presence of more or larger microvoids, which offer more

space for interstitial oxygen. This can explain the reduction of the steady-state refractive index as well as the reduction of the refractive index at the interface. Somehow, the growth of sample C7 differed from all other depositions.

Unexpectedly, a comparison between the N and C sample sets reveals that the reduction of the refractive index is stronger for the N samples. Since the flux ratios were chosen to approximately match the total number of oxygen atoms inside the PECVD plasma and hence a comparable amount of oxygen was available during deposition, one would expect from the oxygen content alone a similar refractive index. In [35] it was found that the refractive index is a mostly linear function of the silicon concentration. From this observation it is clearly understandable that the refractive index of the a-SiO_xN_y samples is lower than the one of the a-SiO_x layers. The silicon concentration is reduced by the additional nitrogen in the a-SiO_xN_y layers, while there is no such significant carbon incorporation for the a-SiO_x layers (see Section 3.1).

In summary, beside the expected reduction of the steady-state refractive index with increasing R_x due to a lower silicon concentration in the layers, the reduction of the refractive index at the interface suggests a less dense microstructure, probably accompanied by microvoid formation, and hence a less ordered amorphous network with increasing R_x, as it was also concluded from the FTIR discussion in Section 3.1. The observed reduction of the refractive index is accompanied by a reduction of the extinction coefficient for wavelengths < 500 nm, which consequently reduces parasitic absorption compared to a pure a-Si:H standard SHJ cell.

3.3. SPV spectroscopy

Fig. 6 shows the SPV spectra of the N and C sample sets acquired with the QTH lamp. A slight slope change at around 1.05–1.09 eV is observable in the spectra of the samples deposited at higher flux ratios R_x (N9.1, N13, N16.6, C9.1), which is related to the band-to-band transition in the c-Si substrate (transition (1) in Fig. 1). In the spectral range of the QTH lamp the light penetration depth, which equals the inverse of the absorption coefficient, is comparable with the whole sample thickness [36] and hence the c-Si band gap is observable. Above the c-Si band gap, the SPV signal does not decrease for all samples, indicating a low interface recombination similar to the as-deposited sample in Fig. 2. This low interface recombination velocity is an indication of a good passivation of the layer, which can be due to chemical passivation and/or charge separation by field effect, as the SPV technique does not allow us to distinguish between these two cases.

The layers deposited at lower flux ratios R_x (N4.8, C4.8, C7 and the reference) show a small signal variation above the c-Si band gap, which can be explained by a low efficiency of the interface potential in separating photo-generated carriers, as SPV signal extraction requires both photon absorption and carrier separation by an electric field. The interface potential is weaker for the layers deposited with lower flux ratios because the band gap discontinuity from the c-Si substrate and the top layer is too small to create an efficient heterojunction capable to separate carriers. This consideration is particularly valid for the pure a-Si:H reference sample.

It must be noted that, unexpectedly, also sample C7 shows an inefficient charge separation, with an overall variation of the signal lower than the one of C4.8, which indicates a reduced electric field at the interface. Such a deviation from the expected trend for the sample C7 was also found in the FTIR and spectral ellipsometry results in Sections 3.1 and Sections 3.2.

Fig. 7 shows SPV spectra acquired with the Xe lamp of both sample sets. Due to the higher photon energy range the light penetration depth is smaller than in the case of the QTH lamp and thus the photoinduced charges are separated mainly by the surface potential and the features of the spectra can be related mostly to the top layers. In the case of the

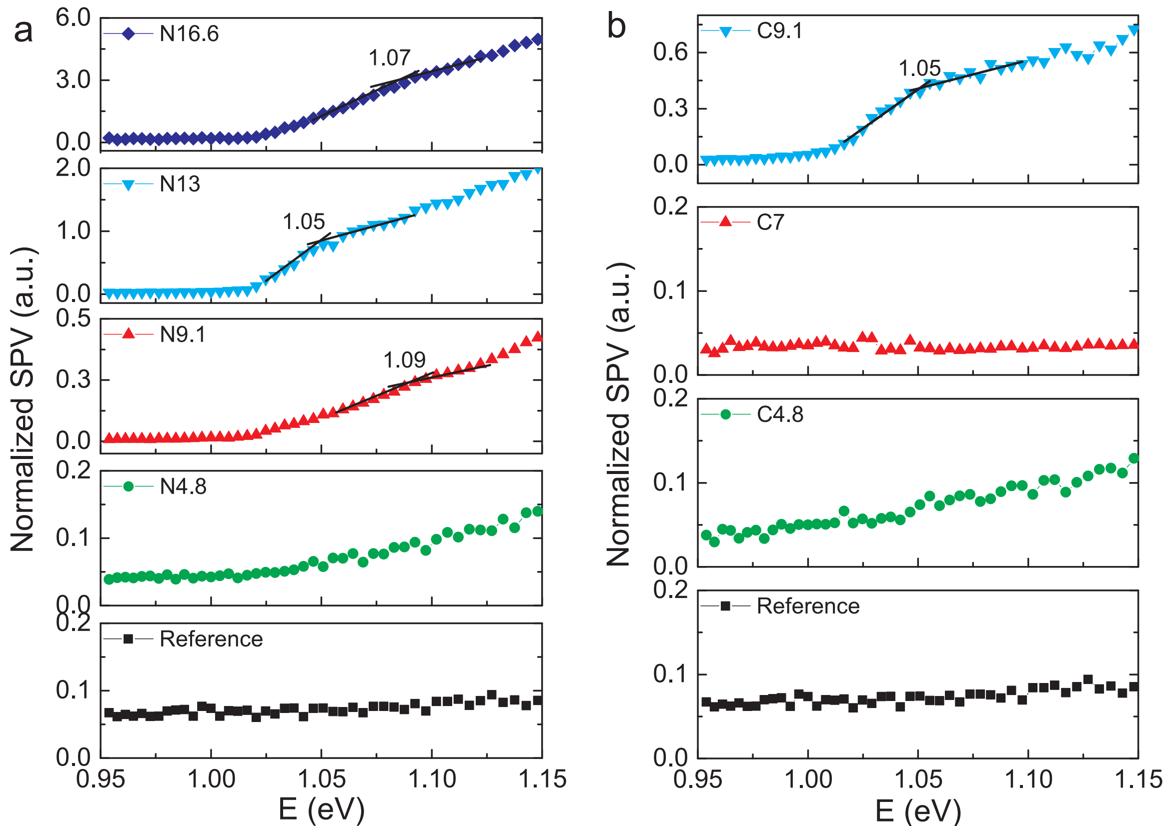

Fig. 6. SPV spectra measured with QTH lamp a) the N sample set and b) the C sample set. The energies (eV) of the relevant features, determined as slope changes in the curves, are marked in the spectra.

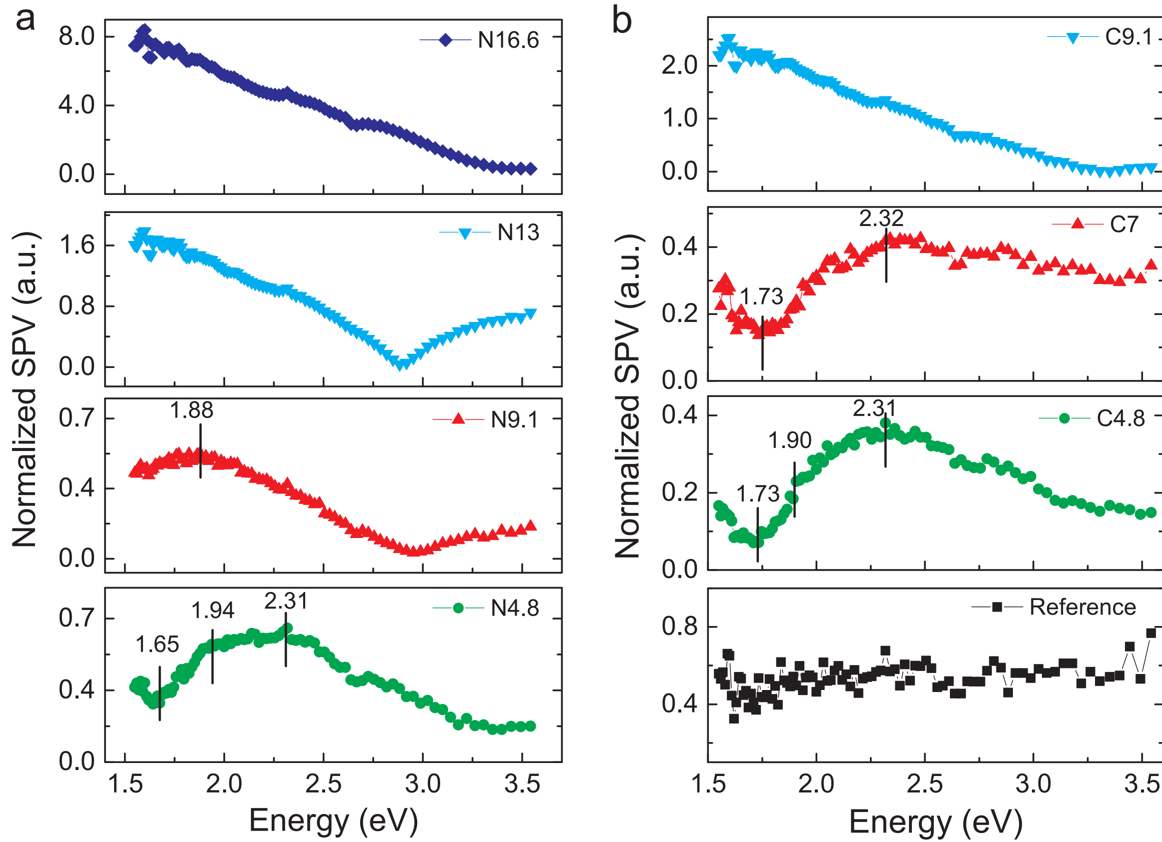

Fig. 7. SPV spectra measured with Xe lamp for a) the N sample set and b) the C sample set. The energies (eV) of the relevant features, determined as slope changes in the curves, are marked in the spectra.

reference sample there is no slope change observable, probably due to a high surface passivation which prevents the surface potential from separating the carriers.

In the spectra of the layers deposited at lower flux ratios R_x three slope changes were found at 1.65–1.73 eV (N4.8, C4.8, C7), at 1.88–1.94 eV (N4.8, N9.1, C4.8) and at 2.31–2.32 eV (N4.8, C4.8, C7). These slope changes in the SPV spectra can be related to the transition from the c-Si valence band to the top layer conduction band (transition (2) in Fig. 1), to the transition from the top layer valence band to the c-Si conduction band (transition (3) in Fig. 1) and to the band-to-band transition in the top layer (transition (4) in Fig. 1), respectively. Following these observations, the effective optical energy gap of the a-SiO_xN_y and a-SiO_x layers is determined to range from 2.30 to 2.32 eV, which is in agreement with previous studies and larger than the energy gap of pure a-Si:H (1.8–1.9 eV), as expected [5,7,37,38].

For the spectra of the layers deposited at higher R_x values (N13, N16.6, C9.1) one would expect a widening of the optical gap and hence a shift of the slope change to values larger than 2.3 eV due to an increased oxygen and nitrogen concentration. However, this expectation could not be tested since none of the three transitions was observable in the spectra of those samples. This behaviour can be attributed to the larger disorder of the amorphous network as it was observed by the FTIR and spectral ellipsometry analyses in Sections 3.1 and Sections 3.2, which induces large tail states in the band gap and eventually causes a significant broadening of the whole spectrum [22].

Beside the observed transitions, a strong signal decrease above the energy gap of the top layer can be observed in all samples apart from the reference, likely related to electron-hole recombination at the top layer surface [22]. Additionally, in the spectra of the samples N13 and N9.1 a further increase of the signal at photon energies larger than 3 eV can be seen. This increase might be caused by a silicon nitride cluster phase, whose energy gap is supposed to be at around 3.2 eV [39,40]. In the spectrum of the sample N16.6 this increase is not visible due to the broadening of the spectrum, as discussed above.

The SPV spectra measured in two distinct spectral ranges allowed for the evaluation of the energy gap of the SiO_xN_y and SiO_x layers deposited at low flux ratios to roughly 2.3 eV. Furthermore, the determination of the energies of the main electronic transitions and the passivation quality of the interfaces and surfaces was possible.

3.4. Passivation quality by lifetime measurements

In [41] the authors built a model to distinguish between chemical passivation due to the reduction of interface density of dangling bonds and a field effect passivation due to charged defects. Applied to intrinsic a-Si:H, they found beside the chemical passivation through saturation of dangling bonds with hydrogen also a field effect caused by the band offset between crystalline and amorphous silicon. In the following, passivation means a combination of both effects as it was not possible to separate them by means of the applied measurement techniques.

The effective minority carrier lifetimes were determined using ac-SPV (Eq. (1)) as well as PCD. The ac-SPV chopper frequency variation was performed at the photon energy of 2.3 eV, corresponding approximately to the top layer energy gap determined in the previous section. Typically, effective minority carrier lifetimes measured by PCD are much smaller than the ones measured by ac-SPV. The PCD measured lifetimes vary in the range of 1.4–2.9 ms while the ac-SPV measured lifetimes vary in the range of 0.6–9.0 ms. This difference occurs due to the influence of the surface recombination velocity, which affects the lifetime values evaluated by PCD more than the ones obtained by ac-SPV [42]. The lifetime values reported in Fig. 8 show the expected behaviour for the samples with lower R_x values, but the reverse behaviour for the samples with higher R_x values. This anomalous behaviour can be explained considering that the ac-SPV lifetime values

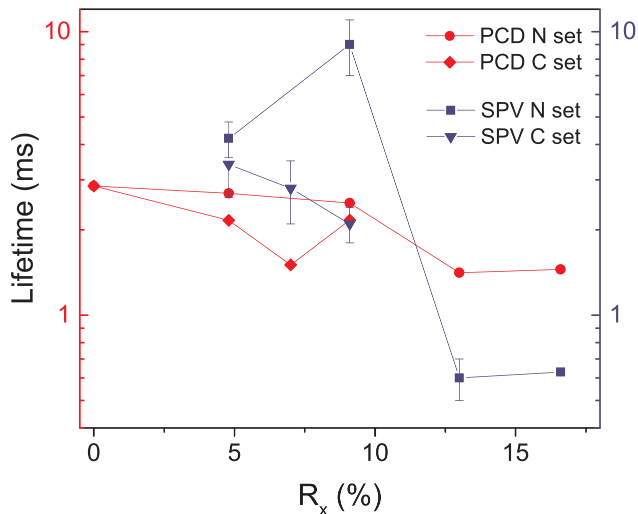

Fig. 8. Effective minority carrier lifetimes measured by PCD and ac-SPV of the N and C sample sets, plotted as a function of the gas flux ratio.

can also be affected by interface recombination, which must be very strong in the samples with higher R_x.

Both techniques show the same overall trend for a reduction in passivation quality with increasing R_x as can be seen in Fig. 8. This is in agreement with the FTIR and spectral ellipsometry results of an increasing disorder of the amorphous network at the interface with increasing R_x (Sections 3.1 and Sections 3.2). However, the detailed results differ between the C and N sample sets as well as between the measurement techniques and thus require clarification.

There is a lack of a clear decreasing trend for the C sample set that show for sample C7 a PCD lifetime of 1.5 ms, which is unexpectedly low compared to 2.2 ms for the sample C9.1. Regarding the FTIR and spectral ellipsometry analyses in Sections 3.1 and Sections 3.2, it was found that the sample C7 deviates from the expected trend due to a large content of interstitial oxygen and a defective amorphous network at the interface. Thus, the lower PCD lifetime of the sample C7 can be explained by a larger interface recombination. It has to be mentioned, that this deviation from a clear trend is not observable for the ac-SPV measured lifetimes.

On the contrary, the effective minority carrier lifetimes of the N sample set show a similar trend between both measurement techniques. Increasing R_{N2O} to values larger than 9.1% leads to a significant drop in lifetime, which suggests the usage of such layers in SHJ cells only in the range of $R_x < 9.1\%$. Precisely, the lifetime values drop from 2.4 ms to 1.4 ms for the PCD measurements and even stronger from 9.0 ms to 0.6 ms for the ac-SPV measured lifetimes. This loss in passivation quality suggests that the sample N13 differs from the expected trend. In the spectral ellipsometry analysis, there was no deviation from the trend found as it was observed for the sample C7. Additionally, the drop in lifetime is similar for both measurement techniques, and hence it cannot be completely attributed to a defective network at the interface. Instead, the reason for this drop can be found in the FTIR results, where the nitrogen content of the sample N13 is larger than expected, i.e. larger than the nitrogen content of sample N16.6. FTIR absorption spectra contain information of the whole layer and if the larger nitrogen content is homogeneously distributed over the whole layer, this might explain that the ac-SPV measured lifetime is also affected.

Additionally, the ac-SPV measured lifetime of the sample N9.1 is anomalously high with a value of 9.0 ms, which is more than twice the value of the sample N4.8 with 4.2 ms. This observation must be linked to an effect of the ac-SPV measurement technique, since no such large deviation from the trend was measured using PCD.

The total reduction in lifetime with increasing R_x is stronger for the N sample set compared to the C sample set, although the flux ratios were chosen to approximately match the total number of oxygen atoms inside the PECVD plasma. Similar to the discussion of the ellipsometry results, this might be a hint that, beside the oxygen content, the additional nitrogen in the N sample set causes an increased amorphous network disorder being responsible for stronger lifetime reduction.

4. Conclusion

The combination of several characterization methods (FTIR, spectral ellipsometry, SPV, PCD) has allowed us to achieve the following conclusions. Both the a-SiO_x and a-SiO_xN_y layers revealed a general similarity in their physical properties. By increasing the flux ratios R_x, the disorder of the amorphous network increases, accompanied by increased Si–H_2 and Si–H_3 bond densities and probably microvoid formation, which is stronger at the interface. The electronic transitions detected by SPV estimated the energy gap of the layers to around 2.3 eV, which is larger than the one of a-Si:H, and thus capable of reducing parasitic absorption. The effective minority carrier lifetimes of the investigated samples show a general decreasing trend for the increase of the flux ratio R_x, which is in agreement with the degradation of the amorphous network evidenced by FTIR and spectral ellipsometry analyses. The anomalous behaviour of the sample C7 has been observed simultaneously with all techniques employed, showing the capabilities of these methods in the analyses of the physical processes involved in the passivation of silicon surfaces and establishing the importance of the approach of using multiple characterization methods in the evaluation of the passivation capability of layers that combine large optical band gap and surface passivation.

We conclude, that the moderate insertion of O and N in a-Si:H, leads to a decrease of optical parasitic absorption, while maintaining the passivation quality of the layers. As generally those layers also show good electrical properties [5–8], they might be successfully applied to improve SHJ solar cell efficiency.

Acknowledgements

We would like to thank Bruna Dudda, master student in Physics at University of Bologna, for the SPV measurements of the annealed samples, Dr Filippo Maria Giorgi, from University of Bologna, for the technical help with the SPV apparatus, and Sibylle Ohl from the University of Konstanz for supporting the layer deposition process.

This research did not receive any specific grant from funding agencies in the public, commercial, or not-for-profit sectors.

References

[1] K. Yamamoto, D. Adachi, K. Yoshikawa, W. Yoshida, T. Irie, K. Konishi, T. Fujimoto, H. Kawasaki, M. Kanematsu, H. Ishibashi, T. Uto, Y. Takahashi, T. Terashita, G. Koizumi, N. Nakanishi, M. Yoshimi, Record-breaking efficiency back-contact heterojunction crystalline Si solar cell and module, in: Proceedings of 33rd Eur. Photovolt. Sol. Energy Conference Exhib, 2017, pp. 201–204.

[2] C. Battaglia, A. Cuevas, S. De Wolf, High-efficiency crystalline silicon solar cells: status and perspectives, Energy Environ. Sci. 9 (2016) 1552–1576, https://doi.org/10.1039/C5EE03380B.

[3] S. De Wolf, A. Descoeudres, Z.C. Holman, C. Ballif, High-efficiency silicon heterojunction solar cells: A review, Green 2 (2012) 7–24, https://doi.org/10.1515/green-2011-0018.

[4] K. Yoshikawa, H. Kawasaki, W. Yoshida, T. Irie, K. Konishi, K. Nakano, T. Uto, D. Adachi, M. Kanematsu, H. Uzu, K. Yamamoto, Silicon heterojunction solar cell with interdigitated back contacts for a photoconversion efficiency over 26%, Nat. Energy 2 (2017) 17032, https://doi.org/10.1038/nenergy.2017.32.

[5] N. Brinkmann, D. Sommer, G. Micard, G. Hahn, B. Terheiden, Electrical, optical and structural investigation of plasma-enhanced chemical-vapor-deposited amorphous silicon oxynitride films for solar cell applications, Sol. Energy Mater. Sol. Cells 108 (2013) 180–188, https://doi.org/10.1016/j.solmat.2012.09.025.

[6] M. Pomaska, J. Mock, F. Köhler, U. Zastrow, M. Perani, O. Astakhov, D. Cavalcoli, R. Carius, F. Finger, K. Ding, Role of oxygen and nitrogen in n-type microcrystalline silicon carbide grown by hot wire chemical vapor deposition, J. Appl. Phys. 120 (2016) 225105, https://doi.org/10.1063/1.4971402.

[7] M. Perani, N. Brinkmann, A. Hammud, D. Cavalcoli, B. Terheiden, Nanocrystal formation in silicon oxy-nitride films for photovoltaic applications: optical and

electrical properties, J. Phys. Chem. C 119 (2015) 13907–13914, https://doi.org/10.1021/acs.jpcc.5b02286.
[8] M.A. Fazio, M. Perani, N. Brinkmann, B. Terheiden, D. Cavalcoli, Transport properties of Si based nanocrystalline films investigated by, J. Alloy. Compd. 725 (2017) 163–170, https://doi.org/10.1016/j.jallcom.2017.07.151.
[9] S. De Wolf, G. Beaucarne, Surface passivation properties of boron-doped plasma-enhanced chemical vapor deposited hydrogenated amorphous silicon films on p-type crystalline Si substrates, Appl. Phys. Lett. 88 (2006) 022104, https://doi.org/10.1063/1.2164902.
[10] S. Dauwe, J. Schmidt, R. Hezel, Very low surface recombination velocities on p- and n-type silicon wafers passivated with hydrogenated amorphous silicon films, in: Conference Rec. Twenty-Ninth IEEE Photovolt. Spec. Conference, IEEE, 2002, pp. 1246–1249 ⟨http://dx.doi.org/10.1109/PVSC.2002.1190834⟩.
[11] S. Heo, J. Lee, S. Heon Kim, D.-J. Yun, J.-B. Park, K. Kim, N. Kim, Y. Kim, D. Lee, K.-S. Kim, H. Jae Kang, Device performance enhancement via a Si-rich silicon oxynitride buffer layer for the organic photodetecting device, Sci. Rep. 7 (2017) 1516, https://doi.org/10.1038/s41598-017-01653-z.
[12] D.M. Zhigunov, A. Sarikov, Y.M. Chesnokov, A.L. Vasiliev, N. Zakharov, P.K. Kashkarov, Thickness and temperature depending intermixing of SiO_x/SiO_2 and SiO_xN_y/SiO_2 superlattices: Experimental observation and thermodynamic modeling, Appl. Phys. Lett. 108 (2016) 223102, https://doi.org/10.1063/1.4953095.
[13] J. Valenta, M. Greben, S. Gutsch, D. Hiller, M. Zacharias, Photoluminescence performance limits of Si nanocrystals in silicon oxynitride matrices, J. Appl. Phys. 122 (2017) 144303, https://doi.org/10.1063/1.4999023.
[14] M. Cardona, Vibrational spectra of hydrogen in silicon and germanium, Phys. Status Solidi 118 (1983) 463–481, https://doi.org/10.1002/pssb.2221180202.
[15] G. Lucovsky, J. Yang, S.S. Chao, J.E. Tyler, W. Czubatyj, Oxygen-bonding environments in glow-discharge-deposited amorphous silicon-hydrogen alloy films, Phys. Rev. B 28 (1983) 3225–3233, https://doi.org/10.1103/PhysRevB.28.3225.
[16] E. Bustarret, M. Bensouda, M.C. Habrard, J.C. Bruyère, S. Poulin, S.C. Gujrathi, Configurational statistics in a-SixNyHz alloys: A quantitative bonding analysis, Phys. Rev. B 38 (1988) 8171–8184, https://doi.org/10.1103/PhysRevB.38.8171.
[17] R. Sčtoudek, J. Humlíček, Infrared spectroscopy of oxygen interstitials and precipitates in nitrogen-doped silicon, Phys. B Condens. Matter 376–377 (2006) 150–153, https://doi.org/10.1016/j.physb.2005.12.040.
[18] H. Shanks, C.J. Fang, L. Ley, M. Cardona, F.J. Demond, S. Kalbitzer, Infrared-spectrum and structure of hydrogenated amorphous silicon, Phys. Status Solidi B-Basic Res. 100 (1980) 43–56, https://doi.org/10.1002/pssb.2221000103.
[19] P.G. Snyder, Y.-M. Xiong, J. Woollam, Graded refractive index silicon oxynitride thin film characterized by spectroscopic ellipsometry, Fac. Publ. Dep. Electr. Comput. Eng. (1992), ⟨https://digitalcommons.unl.edu/electricalengineeringfacpub/69⟩ (Accessed 14 January 2018).
[20] D. Cavalcoli, B. Fraboni, A. Cavallini, Chapter Seven – Surface and Defect States in Semiconductors Investigated by Surface Photovoltage, Defects Semicond. Volume 91, 2015, pp. 251–278. ⟨http://dx.doi.org/10.1016/bs.semsem.2014.11.004⟩.
[21] Y. González, A. Abelenda, M. Sánchez, Surface photovoltage spectroscopy characterization of AlGaAs/GaAs laser structures, J. Phys. Conf. Ser. 792 (2017) 012021, https://doi.org/10.1088/1742-6596/792/1/012021.
[22] L. Kronik, Y. Shapira, Surface photovoltage phenomena: theory, experiment, and applications, Surf. Sci. Rep. 37 (1999) 1–206, https://doi.org/10.1016/S0167-5729(99)00002-3.
[23] D. Cavalcoli, M.A. Fazio, Electronic transitions in low dimensional semiconductor structures measured by surface photovoltage spectroscopy, Mater. Sci. Semicond. Process. (2018), https://doi.org/10.1016/j.mssp.2018.05.027.
[24] T.K. Sharma, S. Kumar, K.C. Rustagi, Frequency and intensity dependence of the sub-band-gap features observed in the surface photovoltage spectrum of semi-insulating GaAs, J. Appl. Phys. 92 (2002) 5959–5965, https://doi.org/10.1063/1.1513203.
[25] J.W. Orton, P. Blood, The Electrical Characterization of Semiconductors: Measurement of Minority Carrier Properties, Academic Press, 1990.
[26] D. Jana, T.K. Sharma, A correlation between the defect states and yellow luminescence in AlGaN/GaN heterostructures, J. Appl. Phys. 122 (2017) 035101, https://doi.org/10.1063/1.4993903.
[27] A.L. Blum, J.S. Swirhun, R.A. Sinton, F. Yan, S. Herasimenka, T. Roth, K. Lauer, J. Haunschild, B. Lim, K. Bothe, Z. Hameiri, B. Seipel, R. Xiong, M. Dhamrin, J.D. Murphy, Interlaboratory study of eddy-current measurement of excess-carrier recombination lifetime, IEEE J. Photovolt. 4 (2014) 525–531.
[28] K.R. McIntosh, R.A. Sinton, Uncertainty in photoconductance lifetime measurements that use an inductive-coil detector, in: 23rd Eur. Photovolt. Sol. Energy Conference, Valencia, 2008, pp. 77–82.
[29] T. Mueller, S. Schwertheim, W.R. Fahrner, Crystalline silicon surface passivation by high-frequency plasma-enhanced chemical-vapor-deposited nanocomposite silicon suboxides for solar cell applications, J. Appl. Phys. 107 (2010) 014504, https://doi.org/10.1063/1.3264626.
[30] A.H.M. Smets, W.M.M. Kessels, M.C.M. Van de Sanden, Vacancies and voids in hydrogenated amorphous silicon, Appl. Phys. Lett. 82 (2003) 1547–1549, https://doi.org/10.1063/1.1559657.
[31] G. Lucovsky, R.J. Nemanich, J.C. Knights, Structural interpretation of the vibrational spectra of a-Si: H alloys, Phys. Rev. B 19 (1979) 2064–2073, https://doi.org/10.1103/PhysRevB.19.2064.
[32] F. Wang, X. Zhang, L. Wang, Y. Jiang, C. Wei, S. Xu, Y. Zhao, Improved amorphous/crystalline silicon interface passivation for heterojunction solar cells by low-temperature chemical vapor deposition and post-annealing treatment, Phys. Chem. Chem. Phys. 16 (2014) 20202, https://doi.org/10.1039/C4CP02212B.
[33] W. Liu, L. Zhang, F. Meng, W. Guo, J. Bao, J. Liu, D. Wang, Z. Liu, Characterization of microvoids in thin hydrogenated amorphous silicon layers by spectroscopic ellipsometry and Fourier transform infrared spectroscopy, Scr. Mater. 107 (2015) 50–53, https://doi.org/10.1016/j.scriptamat.2015.05.018.
[34] T. Bååk, Silicon oxynitride; a material for GRIN optics, Appl. Opt. 21 (1982) 1069, https://doi.org/10.1364/AO.21.001069.
[35] W.R. Knolle, Correlation of refractive index and silicon content of silicon oxynitride films, Thin Solid Films 168 (1989) 123–132, https://doi.org/10.1016/0040-6090(89)90695-0.
[36] W.C. Dash, R. Newman, Intrinsic optical absorption in single-crystal germanium and silicon at 77 K and 300 K, Phys. Rev. 99 (1955) 1151–1155, https://doi.org/10.1103/PhysRev.99.1151.
[37] M. Perani, N. Brinkmann, M.A. Fazio, A. Hammud, B. Terheiden, D. Cavalcoli, Annealing effects on SiOxNy thin films: Optical and morphological properties, Thin Solid Films 617 (2016) 133–137, https://doi.org/10.1016/j.tsf.2016.03.067.
[38] R. Janssen, A. Janotta, D. Dimova-Malinovska, M. Stutzmann, Optical and electrical properties of doped amorphous silicon suboxides, Phys. Rev. B 60 (1999) 13561–13572, https://doi.org/10.1103/PhysRevB.60.13561.
[39] Q.A. Shams, W.D. Brown, Physical and electrical properties of memory quality PECVD silicon oxynitride, J. Electrochem. Soc. 137 (1990) 1244, https://doi.org/10.1149/1.2086640.
[40] V.A. Gritsenko, Electronic structure of silicon nitride, Phys. Uspekhi. 55 (2012) 498–507, https://doi.org/10.1080/01418639108224430.
[41] S. Olibet, E. Vallat-Sauvain, C. Ballif, Model for a-Si:H/c-Si interface recombination based on the amphoteric nature of silicon dangling bonds, Phys. Rev. B 76 (2007) 035326, https://doi.org/10.1103/PhysRevB.76.035326.
[42] N. Honma, C. Munakata, H. Shimizu, Comparison of minority carrier lifetimes measured by photoconductive decay and ac photovoltaic method, Jpn. J. Appl. Phys. 27 (1988) L1498–L1503, https://doi.org/10.1143/JJAP.27.1498.